AJNR

Truncation artifact in MR images of the intervertebral disk.

R K Breger, L F Czervionke, E G Kass, S W Yu, P S Ho, J A Strandt, J B Kneeland and V M Haughton

Truncation Artifact in MR Images of the Intervertebral Disk

Robert K. Breger[1]
Leo F. Czervionke[1]
Edward G. Kass[1]
Shiwei Yu[1]
Peter S. P. Ho[2]
Julie A. Strandt[1]
J. Bruce Kneeland[1]
Victor M. Haughton[1]

A cadaver's vertebral column, a phantom, and a volunteer were imaged on a 1.5-T MR scanner to study the thin, uniform, dark, transverse lines that characterize some intervertebral disks. An artifactual dark line appears when the field of view (FOV) and matrix steps (n) are chosen so that d = FOV/n, where d equals the intervertebral disk height, or spacing between phantom vertebrae. The artifact is caused by the truncation effect. An artifactual dark line is differentiated from a dark line caused by anatomic variables, and means for reducing such lines by modifying imaging parameters are discussed.

The dark transverse bands that have been observed on MR images of the intervertebral disk [1] have variable appearances. Some are characterized by a thick irregular line, some by a narrow regular line. Therefore, we tested the hypothesis that the narrow transverse bands in the disk may represent a "truncation" artifact (Gibb's phenomenon), whose appearance on MR images of other structures has been described [2–6]. The purpose of this paper is to demonstrate the truncation artifact in the intervertebral disk, to discuss briefly its cause, and to suggest methods to minimize the artifact by altering image parameters.

Materials and Methods

The vertebral column excised from a fresh cadaver, a phantom, and a volunteer, were studied by MR.

A thoracic spine was removed en bloc from a frozen, fresh cadaver and a segment containing three intervertebral disks was thawed. The specimen was immersed in a paramagnetic solution (aqueous 0.1 mmol/l copper sulfate [a paramagnetic material]) and imaged with a 1.5-T GE MR scanner. Images were obtained with 128 × 256 and 256 × 256 matrices; 8-, 16-, 20-, and 24-cm fields of view (FOV); 3-, 5-, and 10-mm slice thicknesses; and one, two, and four excitation pulse averages. An intervertebral disk was removed entirely from one level with a scalpel and the spine was immersed in the copper sulfate solution and reimaged. The appearance of the intact spine and the surgically evacuated intervertebral disk spaces was analyzed in relation to field of view, matrix, and intervertebral disk height.

For the phantom, a cylindrical plastic container 16 cm in diameter and 10 cm high was used. The container was filled to a level of 5 cm with either Ringer's lactate solution, distilled water, or the copper sulfate solution, depending on the experiment. Vertebral bodies were modeled with plastic polyethylene containers—3.5 cm in length and width and 5 cm in height—which were filled with commercial household corn oil (Mazola) to simulate fat-containing bone marrow. One to six phantom vertebral bodies were placed in the cylindrical plastic container. Spacing between the phantom vertebrae was varied from 1 to 8 mm. Forty experiments were performed with the phantom in three different sessions. Images were obtained on a 1.5-T GE MR imager with 2500, 500/20, 80 (TRs/TEs); 5- and 10-mm slice thicknesses; contiguous spacing and "skips" of 1, 2, or 5 mm; 8-, 16-, 20-, and 24-cm FOV; 128 × 256 and 256 × 256 matrices; and two or four excitation pulse averages. Artifacts were analyzed in relation to the imaging parameters and spacing of the phantom vertebrae.

With a butterfly surface coil placed under his thoracic spine, a volunteer was placed in a 1.5-T GE MR scanner. Images were obtained in sagittal projection with 2000/60, 20-cm FOV, 128 × 256 matrix, 5-mm slice thickness, and 6-mm intervals. The phase and frequency gradient directions were interchanged and the images repeated with identical parameters.

Results

In these experiments an artifact resembling the so-called intranuclear cleft was produced in the spaces between phantom and cadaver vertebrae. When the 16- or 20-cm field of view and 128 × 256 matrix were used (Figs. 1 and 2), MR showed a dark transverse line in the thoracic intervertebral disk spaces, both those occupied by disk tissue and those in which the salt solution replaced the disk. TR, TE, slice thickness, slice spacing, and number of excitations did not affect the appearance of the artifact, except that no artifact could be detected unless a signal intensity was obtained from the intervertebral disk space.

A similar artifact was also produced in the phantom study.

The artifact, which is typical of the "truncation effect," was demonstrated in images of a single phantom vertebra. Surrounding the single phantom vertebra was a series of evenly spaced bands alternately darker and lighter than the expected signal for the medium. At greater distances from the phantom the bands became less obvious. In images with a 128 × 256 matrix the spacing was greater in the phase-encoding direction (128 steps) than in the frequency-encoding direction. The spacing of the lines was greater when larger FOVs were used (Table 1). When the spacing was measured, it was equal to

$$2 \times \frac{FOV}{n}$$

where n = steps in the matrix (128 or 256). It was not affected by the choice of TR, TE, or medium in which the phantom vertebra was immersed, as long as sufficient signal intensity was returned from the medium. When two or more phantom vertebrae were used, the truncation artifacts between the phantom vertebrae could add or cancel depending on the spacing between them (Fig. 3). The most conspicuous truncation line appeared midway between adjacent vertebral end-
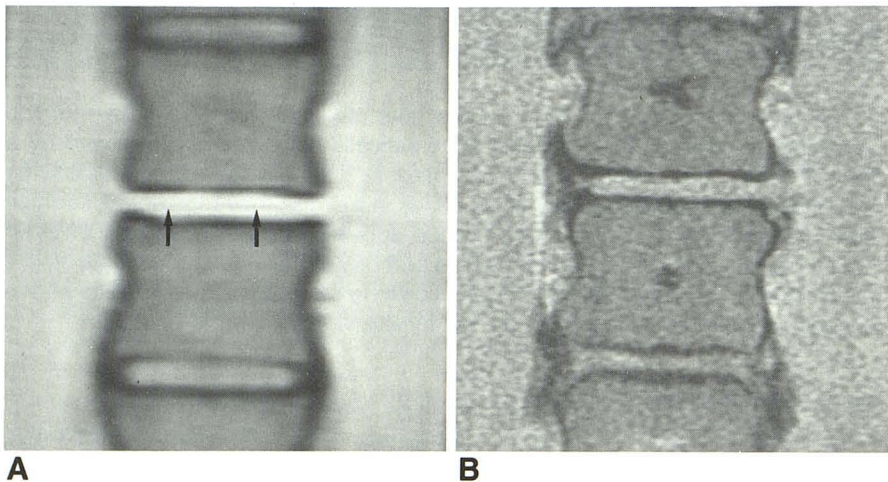

A   **B**

Fig. 1.—*A* and *B*, MR images, coronal plane, through spine specimen with 20-cm (*A*) and 8-cm (*B*) fields of view. Middle intervertebral disk had been removed entirely and specimen immersed in an aqueous solution. Truncation artifact (*arrows*) is evident between endplates in *A* (20-cm FOV, 2000/25) and not apparent in *B* (8-cm FOV, 500/25). In both *A* and *B*, a 128 × 256 matrix was used with phase direction right-left.
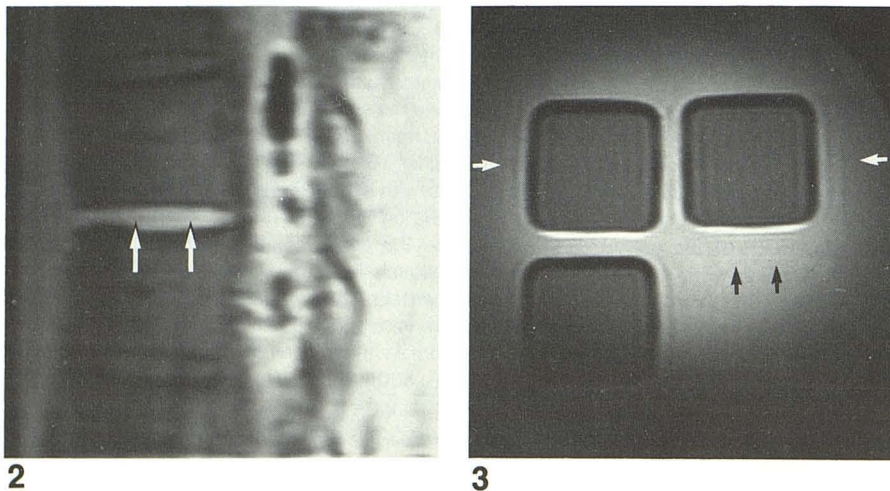

2

Fig. 2.—Sagittal spin-echo image (2500/20) of spine specimen with central disk removed and specimen immersed in an aqueous solution. Note truncation artifact (*arrows*) in fluid-filled disk space. Image obtained with 128 × 256 matrix, phase direction anterior-posterior, and disk spacing 3.2 mm.

3

Fig. 3.—MR image (2500/20) of phantom vertebrae with 128 × 256 matrix and phase direction right-left. Truncation artifacts are broader and more widely spaced along phase-encoding axis (*white arrows*) than in frequency-encoding direction (*black arrows*).

TABLE 1: Empirical Relationships Observed Between FOV, n, and Spacing Between Phantom Vertebrae That Maximized Truncation Artifact in Disk Space

FOV (cm)	Spacing (mm)	
	$n = 128$	$n = 256$
8	2.6	1.3
12	3.8	1.9
16	5.0	2.5
20	6.2	3.1
24	7.6	3.8
32	10.0	5.0

plates in the intervertebral space when the distance (d) between the vertebrae was

$$d = \frac{4 \, FOV}{n}$$

In the volunteer, the dark transverse line in the disk was evident in the images obtained at 24-cm FOV and 128 × 256 matrix with the phase-encoding axis oriented superior to inferior (Fig. 4). It was not evident in the image with the phase and frequency gradients interchanged. The height of the intervertebral disk in the volunteer measured 7 mm.

Discussion

In MR imaging of the spine, truncation artifacts may be seen in several locations [7]. One such artifact appears as a thin dark band extending through the intervertebral disk, mimicking the so-called "intranuclear cleft" [1].

Truncation artifacts (sometimes referred to as Gibb's phenomenon) are produced because Fourier transforms, which are used to reconstruct MR signal data into images on most current MR systems, result in images that imprecisely depict sharp boundaries or interfaces separating regions of high and low signal intensity. Examples of such high-contrast interfaces include the lateral ventricular wall [2], the inner table of the

skull [2], the surface of the spinal cord, the osseous margins of the internal auditory canal [6], and vertebral endplates. These interfaces are most accurately represented in MR images when the Fourier series is very long; however, the Fourier series used for reconstruction is limited; that is, "truncated." Therefore, truncation artifacts are less obvious when a large (e.g., 256 × 256) matrix is selected and more obvious (along the phase-encoding axis) when a 128 × 256 matrix is used [3, 5, 7].

On MR images, truncation artifacts appear as thin bands of alternating low and high signal intensity adjacent to high-contrast interfaces. This fluctuation in signal intensity is represented mathematically by a sine integral function, which is generated in the Fourier transform reconstruction process [7–9].

When two high-contrast interfaces are in proximity (e.g., adjacent vertebral endplates), truncation artifacts produced at each interface cancel or reinforce each other depending on the distance between the interfaces. The most distinct truncation artifacts appear where the truncation artifacts produced at two interfaces maximally reinforce; that is, when the relationship

$$d = 2 \lambda = \frac{4 \, FOV}{n}$$

is fulfilled, where λ is the wavelength of the sine integral function (Fig. 5). In this paper the relationship of d, FOV, and n was determined empirically, but it can be derived mathematically from basic wave theory [3, 5, 7–9]. The truncation artifact between human or phantom vertebral bodies had characteristic features: parallel to the endplates, located precisely midway between the two vertebral endplates, and technique-dependent. They are more commonly seen in thoracic or cervical regions, because of the disk heights.

Truncation artifacts in intervertebral disks can be minimized by one of the following: (1) selecting a large data acquisition matrix, e.g. 256 × 256 or larger; (2) changing the pixel diameter, matrix size, or FOV such that the distance is not equal to 2 λ (four pixels); or (3) filtering the raw data (apodization). Filtering is more useful for MR spectroscopy than for
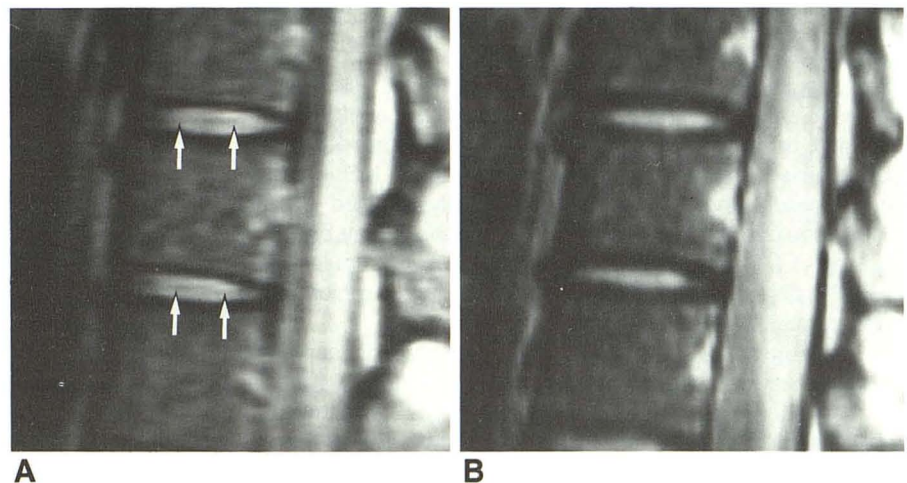

Fig. 4.—A and B, Sagittal spin-echo images (2069/25) of thoracic spine in normal volunteer with the phase (128 steps) superior-inferior (A) and anterior-posterior (B). Thin dark lines in A are characteristic of truncation artifact. The artifact is not apparent in disk when direction of phase-encoding gradient changed to anterior-posterior (B). Both A and B obtained with cardiac and respiratory gating, 128 × 256 matrix, 24-cm FOV, and disk spacing 4 mm.
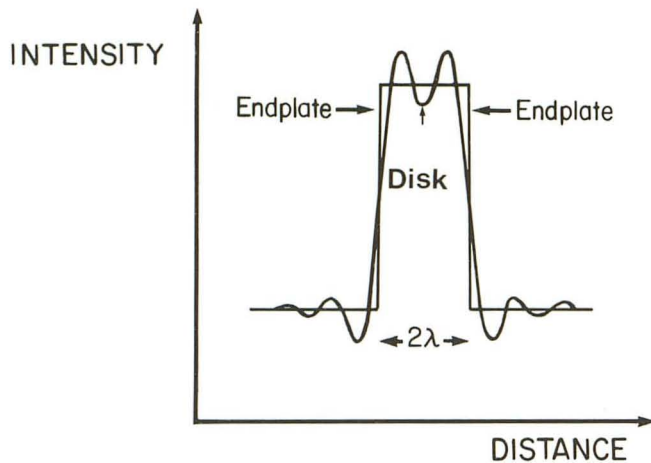
A   B

INTENSITY

Fig. 5.—Plot of signal intensity vs distance across intervertebral disk when fluid is present in the space where truncation artifact is observed. Oscillating sine functions generated at each disk/endplate interface maximally reinforce midway between endplates when separated by a distance of 2 λ.
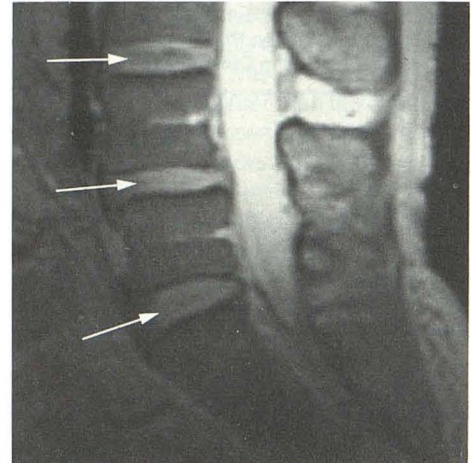

Fig. 6.—MR image (2500/75) shows dark bands (*arrows*) in lumbar disks not explained by truncation artifact. These bands, thicker and coarser than truncation artifacts, represent so-called "intranuclear cleft" (phase direction anterior-posterior, 128 × 256 matrix).

MR imaging, since it results in significant loss of spatial resolution (causing image blurring).

The truncation artifact in the disk can be distinguished from other artifacts. Truncation artifacts are thin, uniform, and located midway between the vertebral endplates. Intranuclear clefts related to true anatomic structure of the disk are broader, less distinct, and less regular. Chemical-shift effects [10, 11] may produce artifactual dark or light bands. Unlike truncation artifacts they are adjacent to vertebral endplates and related to the frequency-encoding axis. Chemical-shift artifacts do not occur midway between the vertebral endplates. Motion artifacts [12–14] related to the CSF pulsation are propagated along the phase-encoding axis as streaks or "ghosts" of abnormal signal intensity. These are propagated throughout the entire image, whereas truncation artifacts diminish in signal intensity with increasing distance from high-contrast interfaces.

The regular dark line caused by truncation must be distinguished from various other dark lines caused by the inhomogeneous structure of the disk (Fig. 6). Irregular bands, not precisely equidistant from the adjacent endplates, indistinctly marginated, are caused by the collagenous "skeleton" of the disk (unpublished data). Although the term intranuclear cleft has been applied to these lines [1], they are not anatomically confined to the nucleus and are not characterized by a physical cleft. Vacuum phenomenon appears in MR images as an irregular region of signal void, usually confined to the nucleus pulposus [15]. The primitive notochord may be recognized in MR images of a newborn as a dark, regular line [16]. Calcification in the disk may also produce a region that appears dark in MR images [17].

In this study the appearance of the truncation artifact in the intervertebral disk was characterized such that the artifact can be distinguished from anatomic structures. The physical explanation of the truncation artifact and Gibb's phenomenon is discussed in more detail elsewhere [7].

REFERENCES

1. Aguila LA, Piraino DW, Modic MT, Dudley AW, Duchesneau PM, Weinstein MA. The intranuclear cleft of the intervertebral disk: magnetic resonance imaging. *Radiology* **1985**;155:155–158
2. Pusey E, Lukin RB, Brown RJ, et al. Magnetic resonance imaging artifacts: mechanism and clinical significance. *Radiographics* **1986**;6:891–911
3. Wood ML, Henkelman RM. Truncation artifacts in magnetic resonance imaging. *Magn Reson Med* **1985**;2:517–526
4. Czervionke LF, Daniels DL, Ho PSP, et al. The MR appearance of gray and white matter in the cervical spinal cord. *AJNR* **1988**;9:557–562
5. Haacke EM. The effects of finite sampling in spin-echo or field-echo magnetic resonance imaging. *Magn Reson Med* **1987**;4:407–421
6. Daniels DL, Czervionke LF, Breger RK, et al. "Truncation" artifact in MR images of the internal auditory canal. *AJNR* **1987**;8:793–794
7. Czervionke LF, Czervionke JM, Daniels DL, Haughton VM. Characteristic features of MR truncation artifacts. *AJNR* **1988**;9:815–824
8. Schenck JF, Hart HR, Foster JH, Edelstein WA, Hussain MA. High resolution magnetic resonance imaging using surface coils. *Magn Res Ann* **1986**;123–160
9. Bracewell RN. *The Fourier transform and its applications*. New York: McGraw-Hill, **1978**
10. Haughton VM, Prost R. Pituitary fossa: chemical shift in MR imaging. *Radiology* **1986**;158:461–462
11. Daniels DL, Kneeland JB, Shimakawa A, et al. MR imaging of the optic nerve and sheath: correcting the chemical misregistration effect. *AJNR* **1986**;7:249–253
12. Rubin JB, Enzmann DR. Optimizing conventional MR imaging of the spine. *Radiology* **1987**;163:777–783
13. Enzmann DR, O'Donohue J, Rubin JB, Shoer L, Cogen P, Silverberg G. CSF pulsations within nonneoplastic spinal cord cysts. *AJNR* **1987**;8:517–526
14. Rubin JB, Enzmann DR. Harmonic modulation of MR precessional phase by pulsatile motion: origin of spinal CSF flow phenomenon. *AJNR* **1987**;8:307–318
15. Grenier N, Grossman RJ, Schiebler ML, Yeager BA, Goldberg HI, Kressel HY. Degenerative lumbar disc disease: pitfalls and usefulness of MR imaging in detection of vacuum phenomenon. *Radiology* **1987**;164:861–865
16. Ho PSP, Yu S, Sether LA, Wagner M, Ho KC, Haughton VM. The progressive and regressive changes in the nucleus pulposus: part I: the neonate. *Radiology* (in press)
17. Ho PSP, Ho KC, Yu S, et al. Calcification of the nucleus pulposus in a premature newborn with pathologic confirmation. *AJNR* (in press)